CALPHAD: Computer Coupling of Phase Diagrams and Thermochemistry 81 (2023) 102531

Contents lists available at ScienceDirect

Calphad

journal homepage: www.elsevier.com/locate/calphad

Reassessment of low-temperature Gibbs energies of BCC and FCC in steel for T_0-temperature evaluation

Aurélie Jacob [a,b,*], Erwin Povoden-Karadeniz [a,c], Philipp Retzl [c,d], Ernst Kozeschnik [d]

[a] Christian Doppler Laboratory for Interface and Precipitation Engineering, Institute of Materials Science and Technology, TU Wien, Getreidemarkt 9, 1060, Vienna, Austria
[b] Materials Center Leoben Forschung GmbH, Roseggerstraße 12, 8700, Leoben, Austria
[c] MatCalc Engineering GmbH, Gumpendorferstraße 21, 1060, Vienna, Austria
[d] Institute of Materials Science and Technology, TU Wien, Getreidemarkt 9, 1060, Vienna, Austria

ARTICLE INFO

Handling Editor: Prof. Z.K. Liu

ABSTRACT

In this work, we present an improved thermodynamic modeling of the mc_fe multicomponent database on the Fe-rich side at low temperatures. This is of special interest for the prediction of bainite and martensite start temperatures. The Fe–Ni, Fe–Mn, and Fe–Cr subsystems of the Fe–Al–C–Cr–Mn–Ni–Si steel system are reassessed with particular focus on the magnetic contributions to Gibbs energies. Moreover, the predicted C dependence of the T_0 line in various extensions of the Fe–C system needed improvement, which is realized by the revision of the Fe–C base in terms of the solubility limit of C in ferrite (BCC). Ternary system descriptions are adapted to the changes made in the binaries.

1. Introduction

Bainite and martensite are metastable steel microstructures occurring in the course of the decomposition of austenite (γ) at low temperatures. They have unique properties and are of high technological importance, and computational prediction of the respective microstructures and their evolution is thus of particular interest. Over several decades, researchers have aimed to model the thermodynamics and kinetics of these transformations [1–4]. The T_0-temperature represents an important pre-requisite. It was proposed by Kaufman and Cohen [5] for the case of a diffusionless transformation. T_0 is the temperature where the Gibbs energy of the parent phase is equal to the one of the product phase and both phases have identical chemical composition. The T_0 – concept postulates that the bainite and martensitic microstructure can only nucleate below the T_0 line in any binary or in the multicomponent steel phase diagram. When considering the bainite growth to be a displacive transformation mechanism, and when considering that the transformation itself involves elastic stresses and plastic strain [6], the start temperature obtained from thermodynamic modeling can also be derived from T_0 and is then called T_0'. T_0' takes the required stress and strain, to make the transformation occur, into account.

Ghosh and Olson [1] proposed a multi-component Fe-base thermodynamic database based on the Calphad method for metastable steel matrix transformation products, which they named kMart. Unfortunately, the parameters of the kMart database were never published. After comparisons of thermodynamic computations with experiments (i.e. heat of transformation, magnetic moment and Curie temperature …), these data seem to represent the most reliable low-temperature Gibbs energy, though. As shown by Ghosh and Olson [1], correct modeling of the magnetism is the key to a successful thermodynamic representation of the Gibbs energy at low temperature due to its impact on the chemical driving force and, thus, a correct representation of the T_0-temperature. Recently, Chen et al. [7] proposed a reassessment of magnetic parameters for their prediction of martensitic start temperatures employing a semi-phenomenological model based on dilatometry within the system Fe–C–Mn–Ni–Si–Cr, which is also within the scope of our interest. However, they did not provide the parameters of their Calphad reassessment, either. Palumbo reviewed [2] the accessible data for martensite start temperatures for steel and shape memory alloys based on Calphad. Borgenstam et al. [8] reviewed the calculation of low temperature martensitic transformation in binary systems, such as Fe–Ni, Fe–Cr, …, etc, and they show that there are discrepancies in terms of the predicted martensitic start temperatures, using the SGTE database available at this time. The difference between experimental data and

* Corresponding author. Christian Doppler Laboratory for Interface and Precipitation Engineering, Institute of Materials Science and Technology, TU Wien, Getreidemarkt 9, 1060, Vienna, Austria.
E-mail address: aurelie.jacob@tuwien.ac.at (A. Jacob).

https://doi.org/10.1016/j.calphad.2023.102531
Received 9 December 2022; Received in revised form 13 January 2023; Accepted 28 January 2023
Available online 8 March 2023

prediction became particularly larger when the alloying content was increased. This inevitably influences also the multi-component steel extensions.

In the present work, the multi-component mc_fe [9] (mc stands for MatCalc [10]) database, version 2.060 [11], is reassessed for its use for martensite and bainite simulations. This database is freely accessible and published under the Open Database License (http://opendatacommons.org/licenses/odbl/1.0/). For physical consistency, the extension of phase stabilities to higher temperatures are also considered in the reassessments. The present work aims to provide a consistent multi-component database specifically designed for thermo-kinetic calculations involving bainite and martensite.

1.1. Thermodynamic modeling

1.1.1. Calphad modeling

Calphad, standing for Calculation of Phase Diagrams, is a versatile method [12] to calculate phase equilibria in multi-component systems and is in the background of software packages for kinetic simulation, such as, Matcalc [10], Dictra&Prisma [13], JMatPro [14], and Pandat [15]. Binary system descriptions play a decisive role for the correct physical extension to multi-component steel thermodynamics and transformation kinetics. In the present work, the update of thermodynamic modeling at low temperatures is done on the solution phases FCC, BCC, and HCP, unless otherwise specified. The molar Gibbs energy of solution phases is given according to the equation:

$$G_m^{\varphi} = \sum x_i^{\varphi 0} G_i^{\varphi} + RT \sum x_i^{\varphi} \, ln\left(x_i^{\varphi}\right) + {}^{magn}G^{\varphi} + {}^{ex}G_m^{\varphi} \tag{1}$$

where ${}^{0}G_i^{\varphi}$ is the Gibbs energy of the pure elements in its reference state and is taken from the standard SGTE database [16]. The second term including temperature dependence is the ideal entropic contribution ($RT\sum x_i^{\varphi} \, ln(x_i^{\varphi})$) to the Gibbs energy. The last two terms are the essence of the Calphad modeling. The term ${}^{magn}G^{\alpha}$ (Eq. (1)) represents the magnetic contribution. Particularly at low temperatures, it plays an important role [1]. The ${}^{ex}G_m^{\varphi}$ represents the excess Gibbs energy of mixing within a solution phase, which describes the deviation from the ideal mixing behavior.

One challenge for the applicability of Calphad-assessed multi-component databases to thermokinetics is to provide physics-based excess energy terms that well represent thermodynamic properties and phase equilibria for a wide range of alloy compositions from low to high temperature. The excess Gibbs energy is modeled by the following Redlich-Kister polynomial, given for a binary system (Eq. (2)), as

$${}^{ex}G_m^{\varphi} = x_i x_j \sum_{i=1}^{n} L_{i,j}^{\varphi} \left(x_i - x_j\right)^k. \tag{2}$$

L is a binary interaction parameter for a phase φ and component i, j and x_i is the mole fraction of component i. k describes the order of the Redlich-Kister polynomial.

In the ternary system, the excess Gibbs energy [17] can be written as:

$${}^{ex}G_m^{\varphi} = \sum_{i=1}^{n-2} \sum_{j>1}^{n-1} \sum_{z>j}^{n} x_i x_j x_z \left(L_{i,j,z}^{1,\varphi}\left(x_i + \delta_{ijz}\right) + L_{i,j,z}^{2,\varphi}\left(x_i + \delta_{ijz}\right) + L_{i,j,z}^{3,\varphi}\left(x_i + \delta_{ijz}\right)\right). \tag{3}$$

Where

$$\delta_{ijk} = \frac{1 - x_i - x_j - x_z}{3} \tag{4}$$

For the magnetic modeling, several models exist. In the present work, we use the Inden-Hillert-Jarl [18] model following the equation:

$${}^{magn}G^{\varphi} = RTln(B^{\varphi} + 1) f(\tau^{\varphi}). \tag{5}$$

We use this 2nd generation Calphad model because the application of newer approaches to the magnetic modeling for simulations in multi-component steel is not yet satisfying. It is emphasized, though, that the chosen older model is not incorrect and possible limitations, for instance in the precise predictions of physics of magnetic behavior, which would require using a more advanced approach, lie outside of our present database application to martensite and bainite transformations. In the Inden-Hillert-Jarl model, just like the excess Gibbs energy, the magnetic contribution, B^{φ} and τ^{φ}, representing the magnetic moment in the form of Bohr magneton, and the Curie temperature, $T_{c,}$ respectively, can be adjusted and optimized according to experimental or DFT evidence. Empirical magnetic interactions between elements in a solution phase, thus alloying to match B^{φ} and τ^{φ} in multi-component systems, can be expressed by Redlich-Kister polynomials. A comprehensive discussion of the magnetic parameters is given, for instance, in Ref. [1]. In the context of the thermodynamic modeling of bainite and martensite start temperature, it has already been shown that the magnetic contribution has not been well modeled, for instance, in Fe-Ni [1,19]. Therefore, the resulting low temperature region of the phase diagram is doubtful [1,2,19–21] in terms of the computed thermodynamic properties and, thus, also T_0 derived from them (see Eq. (6) below, section I.c).

Table 1
List of Fe-containing sub-systems of consideration with their original references in the mc_fe database.

Systems	Original work used in mc_fe [9]	Critically reviewed	Comments
Fe–Ni	Gabriel et al. [22]	Cacciamani et al. [20] Ohnuma et al. [23] Xiong et al. [19]	Re-optimization of magnetic contributions
Fe–Mn	Huang et al. [24]	Bigdeli et al. [21]	Re-optimization of magnetic contributions and metastable HCP.
Fe–Cr	Andersson et al. [25]	Xiong et al. [26,27] Jacob et al. [28] Lafaye et al. [29]	Revision of magnetic contribution, reassessed by Jacob et al. [28]
Fe–Si	Lacaze et al. [30]	Ohnuma et al. [31] Yuan et al. [32] Cui et al. [33]	Shift parameters back to Lacaze et al. [30]
Fe–Al	Saunders et al. [34]		Updated to Rank et al. [35]
Fe–C	Gustafson [36]	Naraghi et al. [37]	Optimized to improve the slope of T_0 in multi-component extensions

1.1.2. Literature assessment

In the present work, the elements of interest are C, Ni, Mn, Cr, Al, and Si in Fe-based alloys. The multi-component thermodynamic database mc_fe, version 2.060 [9,11], is reassessed, because it is published under the Open Database License (http://opendatacommons.org/licenses/odbl/1.0/) and it can, therefore, be freely used and optimized.

Revision may be required due to inconsistencies of the previously assessed phase boundaries or thermodynamic properties with available experimental data, or new data due to more recent papers, including DFT calculations. To provide an overview, Table 1 lists all Fe-containing binaries of the considered steel system, their modeling in mc_fe, further key papers for the respective system, and comments on the performed type of re-optimization in the present study.

1.1.3. Thermodynamic modeling of T_0

First, some fundamental concepts of the transformation from austenite to bainite and martensite and their links to Gibbs energy are defined. T_0 is the temperature, where the Gibbs energy of the parent

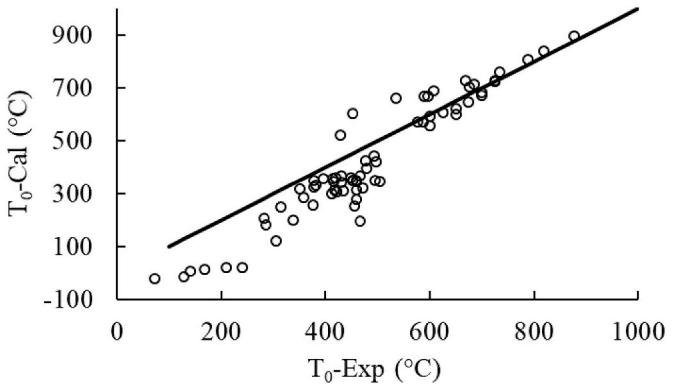

Fig. 1. Calculated T_0 from the original mc_fe without re-assessments compared to "experimental" data [40–43].

phase is identical to that of the product phase of the same composition, as defined by Kaufman and Cohen [5]. For the [5] transformation between austenite and ferrite, we obtain

$$G^{\gamma}(T_0) = G^{\alpha}(T_0). \tag{6}$$

Experimentally, this temperature is not directly accessible. Nevertheless, it has previously been simply approximated from the equilibrium austenite solvus temperature (A_s) and the martensite start temperature (M_s) with

$$T_0 = \frac{(A_s + M_s)}{2}. \tag{7}$$

Derivation of Eq. (7) can be found in Ref. [2]. It represents the thermodynamic limit for a diffusionless transformation [4]. According to Kaufman and Cohen [5], this equation can be apply in Fe-based systems as the difference between A_s and M_s is sufficiently high, i.e. ~400 °C not to be influenced by strain energy. The M_s temperature may in fact be influenced by the strain energy in case of the too low difference with A_s which then could promote a prematurely reverse transformation and thus bias the indirect characterization of T_0. For simplicity, we denote the resulting T_0 from this relation as "experimental", in the following, although it is actually derived from A_s and M_s.

From Eq. (7), it is clear that the accuracy of a T_0 prediction depends on the correct representation of the Gibbs energies of parent and product phases. In the context of modeling bainitic and martensitic transformations, it was shown that improvement of the modeling representation of magnetic phase transitions [1,7] can also help to improve the representation of the low temperature phase equilibria. This goes hand in hand with a more accurate representation of the T_0 and bainite and martensite start temperatures, which all are influenced by them.

The bainitic and martensitic start temperatures are calculated via the T_0 concept by including the strain energy E_{str} involved in the transformation,

$$G^{\gamma}\left(T_0^{Bs,Ms}\right) = G^{\alpha}(T_0) + E_{str} \tag{8}$$

where B_s and M_s are the bainite and martensite start temperatures, respectively. The value of E_{str} depends on the type of transformation. For bainitic transformation, 400 J mol^{-1} has been proposed and the corresponding temperature is called T_0' [6], for martensite it is $1200 < E_{str} < 1700$ J mol^{-1} [38]. Further discussion on this additional strain-related term will be given in a follow-up publication focusing on the prediction of bainite start temperatures [39]. In the following, our focus is on the improvement of the Calphad base for correct predictions of T_0 temperatures. In Fig. 1, a comparison of "experimental" and computed T_0 temperatures using mc_fe, without reassessment, for various sub-systems is shown.

The calculation of T_0 shows good agreement at higher temperatures but increasing deviations compared to experiments at temperatures below 500 °C. This concerns the system Fe–Ni, Fe–Cr, and their ternary extensions to the combination with C, Si, Al, and Mn.

1.2. Thermodynamic reassessment of binary sub-systems

1.2.1. Fe–Ni

In mc_fe, the first Fe–Ni assessment from Gabriel et al. [22] has been adopted. However, several reassessments appeared since the original publication [19,20,23]. In Fig. 2, the reproduction of the critical low to intermediate temperature region of the pure Fe–Ni BCC-FCC system without intermetallic phases (mimicking a pure alloy matrix phase transformation), and the critical thermodynamic property for bainitic and martensitic transformations, T_0, as obtained by different publications (experimental - symbols and modeling - lines), is shown.

The thermodynamic modeling of Fe–Ni, as included in mc_fe and based on the parameters of Gabriel et al. [22], shows a too low solubility of Ni in Fe-BCC, which is inconsistent with the most actual experimentally determined phase boundaries in the system [23]. This results in an underestimation of the T_0-temperature (Fig. 2b) compared to other thermodynamic modeling and experiments [1,41,47,48].

Xiong et al. [19] mentioned that the reason for the problematic BCC-FCC *phase boundary compared to experimental data as given by Gabriel* et al. [22] has been an unfortunate choice of the magnetic model parameters, which has been accepted by the community until recently [19,20,23]. They proposed a reassessment of the system based on their new

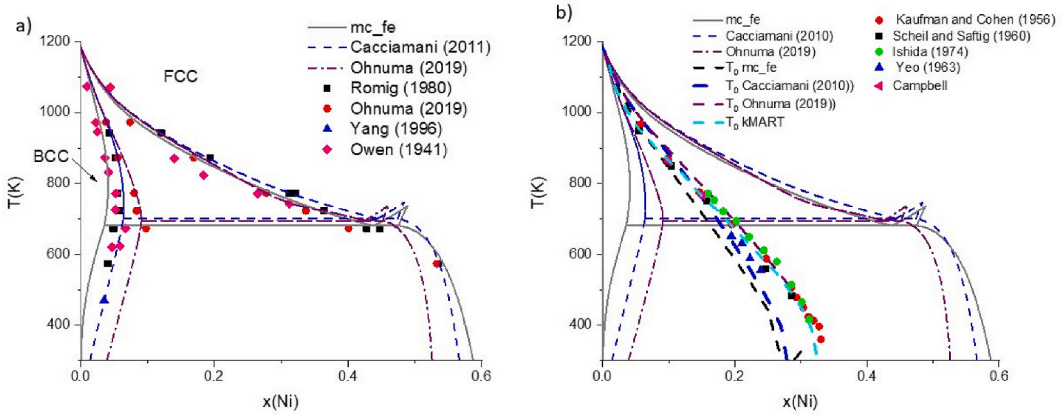

Fig. 2. Calculated Fe–Ni low and intermediate temperature phase diagram including only FCC and BCC (thus mimicking pure matrix transformation) a) Alloy phase equilibria [14,17,20] compared to experimental data [23,44–46] and according to T_0 calculations, compared to experiments from the literature [1,41,47,48]. The original data of Campbell were taken from Ghosh and Olson [1].

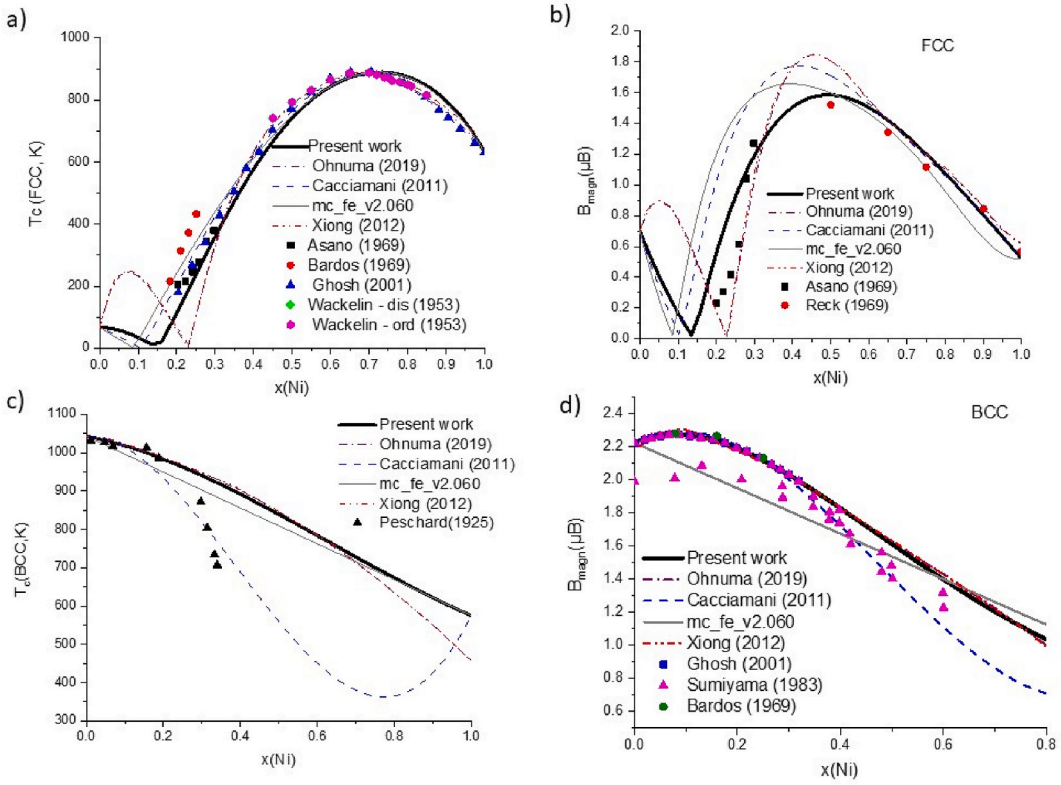

Fig. 3. Magnetic properties of FCC and BCC in the Fe–Ni according to the present modeling a) T_c(FCC) b) B^{FCC}_{magn} c) T_c(BCC) d) B^{BCC}_{magn} compared with thermodynamic modeling from Refs. [9,19,20,23] and experimental data [1,50–55].

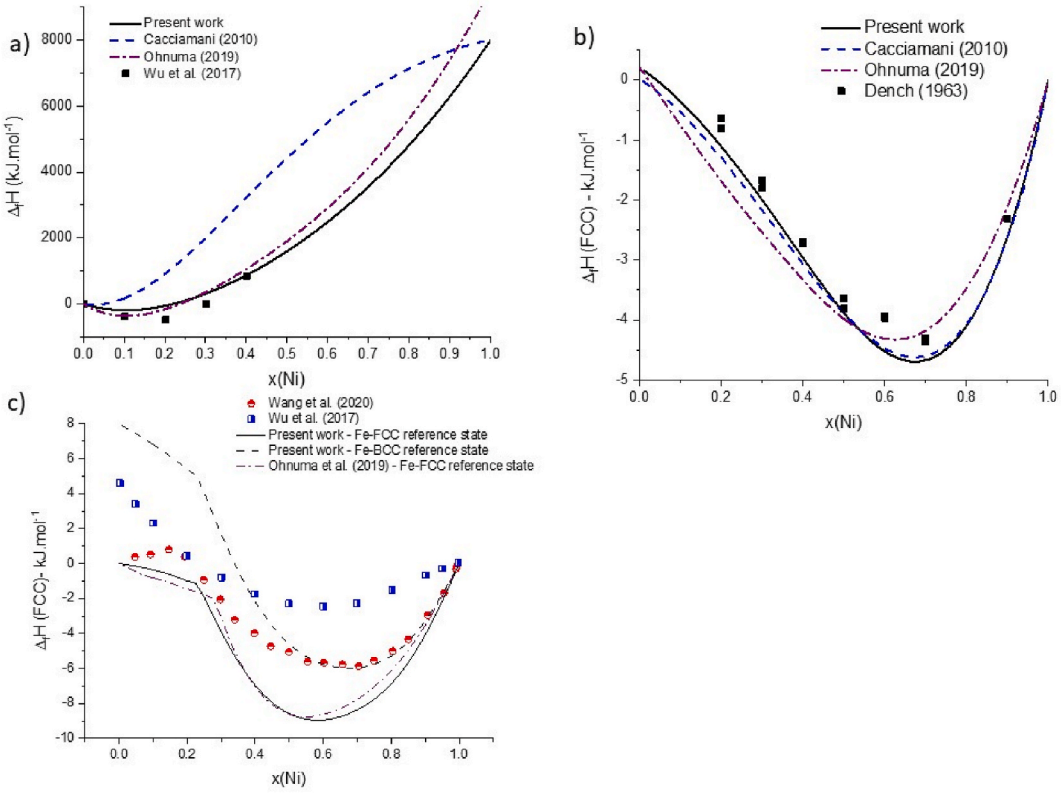

Fig. 4. a) Enthalpy of formation of BCC at T = 298 K compared to interaction potential calculations from Wu et al. [56] with SER reference, b) Comparison with experimental data from Dench et al. [57] at T = 1050 °C and c) Comparison with DFT data [56,58] at T = 298 K with SER reference.

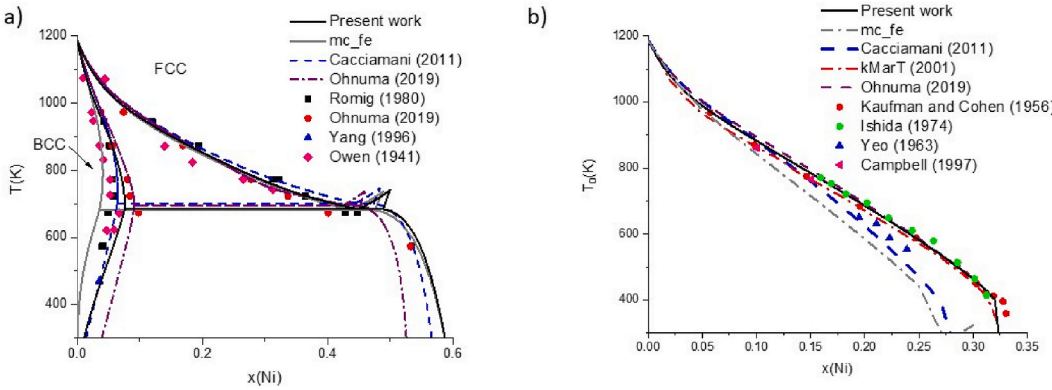

Fig. 5. Optimized Fe–Ni compared to previous work and experiments and T_0 calculation compared to experiments [41,48,59,60].

magnetic model [49] and 3rd generation description of the pure elements. We determined the appropriate B_{magn}^{FCC}, and re-adjusted the magnetic model parameters, which control the Curie temperatures for FCC and BCC, employing the 2nd generation magnetic modeling [13] instead. Our results are presented in Fig. 3.

The original work of Gabriel et al. [22] used in mc_fe [9] lacks to represent correctly the magnetic properties of the system. More recent thermodynamic modeling, such as the one of Cacciamani et al. [20], is diverging from the experiments on B_{magn}^{FCC} (see Fig. 10b of the original paper). Xiong et al. [19] pointed out this problem and reassessed and optimized the system using a new description of the pure elements based on the third generation Calphad database description and optimized the binary introducing more interaction parameters to describe B_{mag}. It seems that the model parameters offered by Xiong et al. [19] provide a more consistent representation of experiments compared to the previous optimization. Here, we used them as starting points for the present assessment. In the course of our optimization, only the first interaction parameters were adjusted, i.e. $L^0(B_{magn}, FCC)$, and the other parameters were kept as given in the original work of Xiong et al. [19].

According to Xiong et al. [19], their DFT values of the Curie temperature do not support the experimental results of Peschard et al. [55]. It is to be noted that Xiong et al. [19] offered more "experimental data" cited as Peschard's data than can be found in the original work, which contains only three experimental points, lying within the range of the BCC phase stability.

Anyway, in the present work, any attempt to fit the data of Peschard et al. [55] as given by previous thermodynamic modeling [19,20] led to the wrong T_0 (this problem applies most to Cacciamani's parameter choice – best match of Peschard et al.'s data, but too low T_0, Fig. 2b). This supports the decision for low weighing of Peschard et al.'s data in the present reassessment, and our results go along with those of Xiong et al. [19]. Concerning the T_c (FCC), our optimization follows the experimental data of Asano et al. [50], while Xiong et al. [19] are offering lower values.

In our re-optimization, we use three interaction parameters for the excess enthalpies of mixing for both alloy solution phases, different from the ideal mixing approach from Gabriel et al. [19]. The L^0 term of the Redlich-Kister polynomial for BCC and FCC has particular control on the best match with experimental thermodynamic data [48,49]. This is clear, since L^0 represents a symmetric energy modulation in an A-B system, with the strongest effect at 50 at. % B. Though, first and second order interaction parameters were used, as discussed later. The results of enthalpies of mixing are given in Fig. 4.

The enthalpy of mixing of FCC is fitted to the high temperature measurements of Dench et al. [57] at 1050 °C. While our parametrization is consistent with their data, it is not possible to get the same good agreement at low temperatures compared to DFT [56,58]. In their DFT-based Calphad assessment, it should be noted that Wang et al. [58] proposed a Redlich-Kister polynomial to fit their enthalpy of mixing

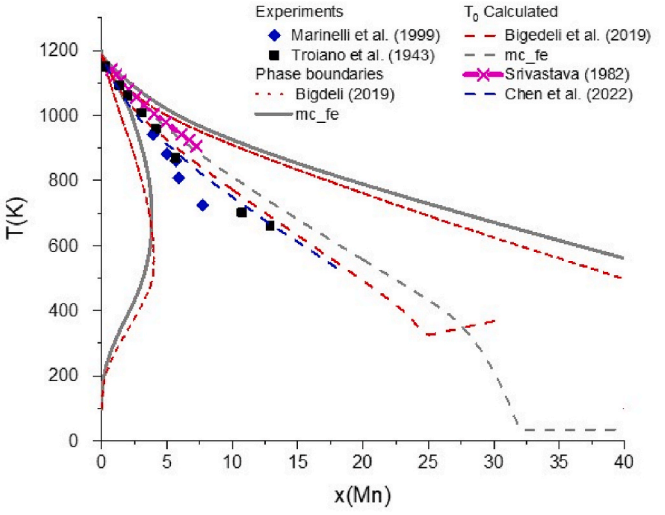

Fig. 6. BCC/FCC low to intermediate temperature phase diagram with the calculated T_0 line (dashed lines) from mc_fe [9,11] of the Fe–Mn system compared to the calculated values of Bigdeli et al. [21], Srivastava et al. [61] and Chen et al. [7], and the experiments of Troiano et al. [42] and Marinelli et al. [43].

with five interaction parameters. In Calphad modeling, the use of so many interaction parameters is not advised, especially, when extrapolated to higher order systems as this might potentially lead to unphysical behavior, such as formations of artificial miscibility gaps. Any attempt to get better consistency in the DFT data leads to strong deviations from the values given by Dench et al. [58] and to a wrong representation of the phase diagram. Therefore, the DFT values were not perfectly fitted to provide consistency with the phase diagram and the experimental enthalpy of mixing.

Optimization of ^1L and ^2L parameters of the Redlich-Kister polynomial had a particular influence on phase boundaries, but they did not strongly affect the H_m curves. In this sense, they provided further consistency between the calculated and experimental phase diagrams, without deteriorating H_m. During the optimization process, it was found that a slight shift of the B_{magn}^{BCC} can significantly affect the slope of T_0. The best results for T_0 and related bainitic start temperatures in multicomponent extensions were obtained by following the same trend of B_{magn}^{BCC} with Ni-alloying as Xiong et al. [19]. It is noticeable that, while it is possible to obtain a suitable representation of the phase diagram, the calculation of T_0 can still substantially vary [41], especially at high Ni content (and thus low temperature), depending on the choice of magnetic parameters. Our thermodynamic description proposes a higher solubility limit of Ni in BCC-Fe than the previous thermodynamic

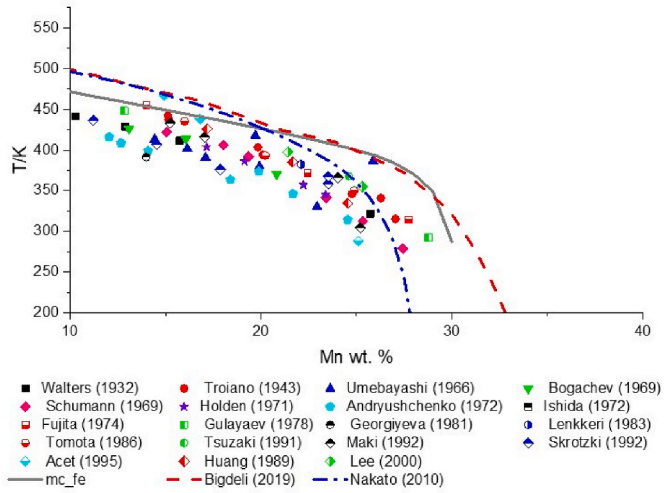

Fig. 7. Calculated T_0 for the transformation of FCC into metastable HCP compared to experiments [62–79] and modeling [9,21,79].

modeling [20,22] and fits better the Ohnuma et al. [23] solubility data. Also, older experimental data from Yang et al. [45] are in agreement with our suggestion for the Ni-solubility in BCC-Fe. Our revised thermodynamic parameter set allows for a T_0 line, which is following the experimental data from low to high Ni content [41,47,48].

1.2.2. *Fe–Mn*

From low and intermediate temperatures at the Fe-rich side, the Fe–Mn system is characterized by the presence of FCC and BCC phases.

There are two types of martensitic transformation in the system, at low Mn content between FCC and BCC, and at concentrations above 10 wt % Mn, the FCC structure transforms into HCP. This transformation is of primary importance for TRIP steels. In mc_fe [9,11], the thermodynamic modeling of Huang et al. [24] has been adopted. The system has been recently re-optimized by Bigdeli et al. [21] using the third generation data of the pure elements to get better reliability of results below 298 K (see Fig. 5).

According to Fig. 6, the T_0 results given by Chen et al. [7] provide better consistency than the optimization of Bigdeli et al. [21]. The results of the present mc_fe [9,11] database are too high compared to the experiments [42,43], thus reassessment is needed. Even though the parameter optimization of Chen et al. [7] is indeed an improvement to the T_0 line of the system, no parameters and no comparison to experimental thermodynamic data have been provided. Therefore, we propose an alternative reassessment here. The results of the mc_fe [9,11] database are too high compared to the experiments [42,43] for a proper reproduction of the T_0 line between FCC and HCP. Aside, it is notable that, because of the development of high-Mn TRIP steel, the description of the HCP stability needs to be improved. The actual trend (mc_fe) of the T_0 line of the FCC to HCP phase transformation as function of x(Mn) is given in Fig. 7 and compared to experimental data (see Fig. 8).

As shown in Fig. 7, the calculated T_0 trend obtained from mc_fe is too flat toward high Mn-content above 20 wt%. Thus, the thermodynamic modeling adopted from Huang et al. [24] in mc_fe has to be reconsidered. This concerns, in particular, the magnetic model parametrizations, which have also been observed in the previously discussed Fe–Ni system.

Witusiewic et al. [82] re-optimized the system based on their experimental data [80]. Their assessment provides better consistency in the C_p calculation of FCC [82] than the previous thermodynamic parameters given by Huang et al. [24]. Nevertheless, their suggestion of the magnetic model is not implemented in the available Calphad software [21] and, thus, cannot be directly used. The most recent optimization given by Bigdeli et al. [21] is not adopted here for the reason already mentioned previously. They used the third generation of the pure element, which is not implemented in MatCalc to date.

For the re-optimization of the Fe–Mn system in the present work we also, as for Fe–Ni, weigh the assessment of magnetic contributions of FCC, BCC, and HCP high, by choosing appropriate Redlich-Kister polynomials for magnetic interactions. This shifted computed T_0 particularly close to the proposed ones for the FCC-HCP transformation (see Fig. 7), while we keep the reproduction of equilibrium phase boundaries in the system.

The revision of the magnetic contribution of the FCC allows getting

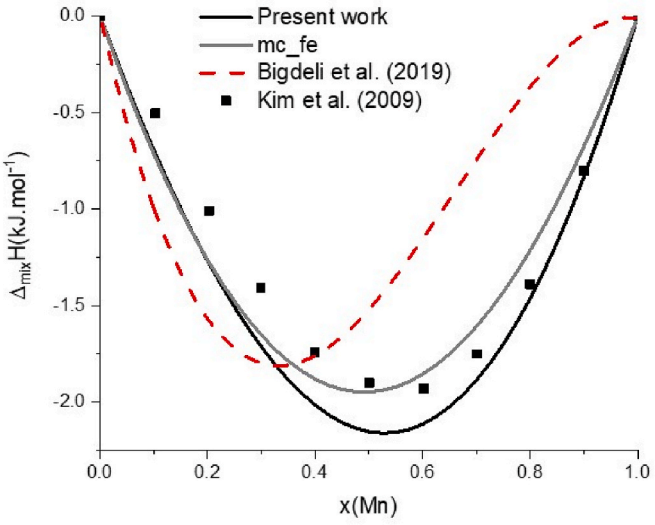

Fig. 9. Enthalpy of mixing of FCC at $T = 1000$ K compared to MEAM [83] and previous thermodynamic modeling [21,24].

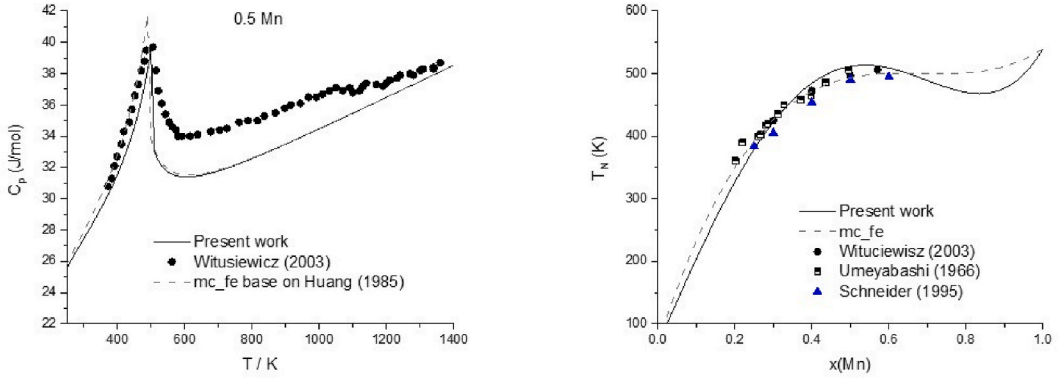

Fig. 8. C_p and T_N of FCC-Fe-Mn compared to previous thermodynamic modeling [24] and experiments [64,80,81].

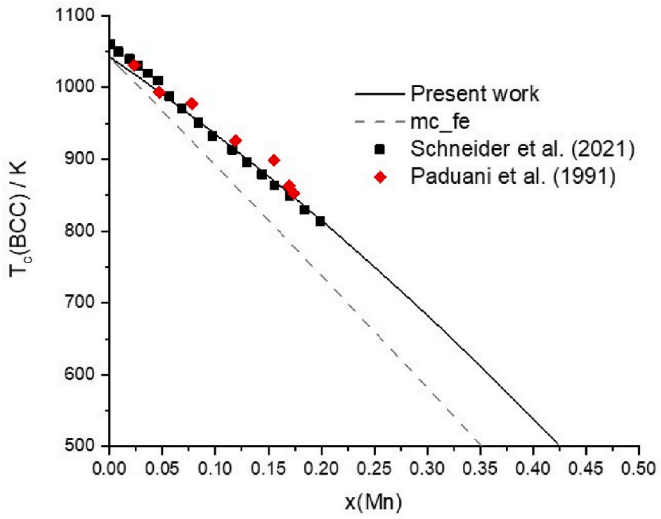

Fig. 10. Calculated Curie temperature of BCC Fe–Mn compared to DFT calculation from Schneider et al. [84], Mösbauer spectroscopy from Paduani et al. [85], and previous thermodynamic modeling [24].

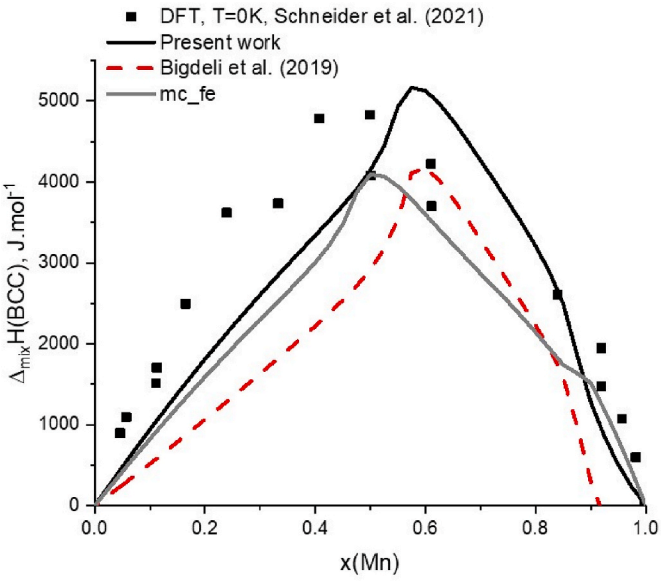

Fig. 11. Calculated enthalpy of mixing of BCC compared to DFT results from Schneider et al. [84] and previous thermodynamic modeling [21,24].

more consistent modeling for the T_0 calculation while the C_p remain similar compared to Witusiewicz et al. [80]. In the following, the result of the mixing enthalpy in FCC (Fig. 9) at 1000 °C is compared to the modified embedded-atom method (MEAM) from Kim et al. [83].

The location of the minimum enthalpy of mixing given by Kim et al. [83] is observed at a slightly higher Mn content than the previous thermodynamic modeling. Our parametrization follows, in general, the results of Kim et al. [83], however with a lower minimum, which allowed for the best agreement between experiments and simulation for the thermodynamic properties, the phase diagram, and the T_0 lines.

From Fig. 10, it is clear that the magnetic model parameters needed to be revised for BCC. The new parametrization led to consistent results with recent DFT [84] and experimental data [85]. We also revised interaction parameters for the BCC phase in the Fe–Mn system to obtain the best match of experimental and DFT enthalpies of mixing (see Fig. 11) and phase boundaries of the phase diagram. In Fig. 12a, the resulting calculated phase diagram is shown. The agreement with experimental data is good. The T_0 lines of BCC/FCC (Fig. 12b) and FCC/HCP (Fig. 12c) are also improved by our reassessment.

Even though the Fe–Mn system has been re-optimized focusing on the revision of the magnetism to provide a most reliable base for the computations of phase transitions at low and intermediate temperatures, the achieved FCC/BCC T_0 line is still slightly higher than the experimental results and the two latest calculations [21,79]. It is notable that T_0 remains a derived property from thermodynamic data, compared to more robust thermodynamic properties, as obtained by calorimetry, and magnetic contributions to the Gibbs energies. Moreover, the experimental data of T_0, as given by Troiano and McGuire [42], lack accuracy due to inconsistent lattice parameters of BCC and FCC, while Marinelli et al. [43] provided questionable M_s (lower M_s temperature as previous studies, see Fig. 2 of the original work). Thus, we justify the difference of the T_0 calculated in the present work compared to experimental findings, since we put a high weight on calorimetrically measurable and magnetic contributions to the Gibbs energies.

1.2.3. Fe–Cr, Fe–Si, and Fe–Al

In mc_fe [9,11], model descriptions of the Fe–Cr system were adopted from the original work of Andersson and Sundman [25]. Recently, there have been several updates to this system. While Xiong et al. [27] remodeled it using the 3rd generation of pure elements, Jacob et al. [87] and Lafaye et al. [29] used the standard SGTE pure elements database. Jacob et al. [87] revised the system completely, particularly by reassessing the miscibility gap and magnetic parameters. Lafaye et al. [29] focused mainly on the σ phase, and no details are given on the thermodynamics of the different phases. Thus, the Fe–Cr assessment from Jacob et al. [87] is used in the assessed multi-component database of this study instead of the data from Andersson and Sundman [25].

The Fe–Si thermodynamic model parameters in mc_fe [9,11] were adopted from the original work of Lacaze and Sundman [30] with the revised liquid description from Miettinen [88]. This system has been re-optimized several times [31–33]. Ohnuma et al. [31] reassessed the systems based on their experiments obtained by deformed particles and solution annealing treatment and provided a consistent dataset for order-disordered transition for the FCC phase in the system. Yuan et al. [89] revised the system but kept the original parameters of Lacaze and Sundman [30] for BCC and FCC phases. The latest optimization of the system was provided by Cui et al. [90] who justified a re-optimization based on the work of Ohnuma [31] as the later one did not properly consider the intermetallic phases. In the present work, we checked the influence of different alloy interactions and magnetic parameters on the calculation of T_0 and calculated B_s in a multi-component environment. It was found that the work of Cui et al. [90] lead to the improvement of the calculation [90] in multi-component systems. Therefore, the parameters of Cui et al. [90] were updated in the present work as previously edited in the mc_fe database.

Al is used as a cementite destabilizer in steel making, in the same way as Si. These two elements thus contribute to carbide-free bainite, and the Fe–Al system is also of interest to the present investigation. In the mc_fe database, parameters were adopted from Saunders [34]. Since this work, there have been several new assessments published [35,91,92]. The optimization of Sundman et al. [91] is widely accepted [93] in multi-component systems but the FCC parameters have been questioned, recently, by Rank et al. [35]. In the present work, we updated the parameters to the most recent ones given by Rank et al. [35] due to the shift of the sublattice model for the intermetallic phases and associated modification of the solution phases. It results in a better shape of the γ-loop, while still using the magnetic contribution from Sundman et al. [91], since calculated B_s are consistent with experimental results from Tian et al. [94].

1.2.4. Fe–C

The Fe–C system is of primary importance for steel, and the optimization of Gustafson [36] is well accepted and widely used in Fe-based

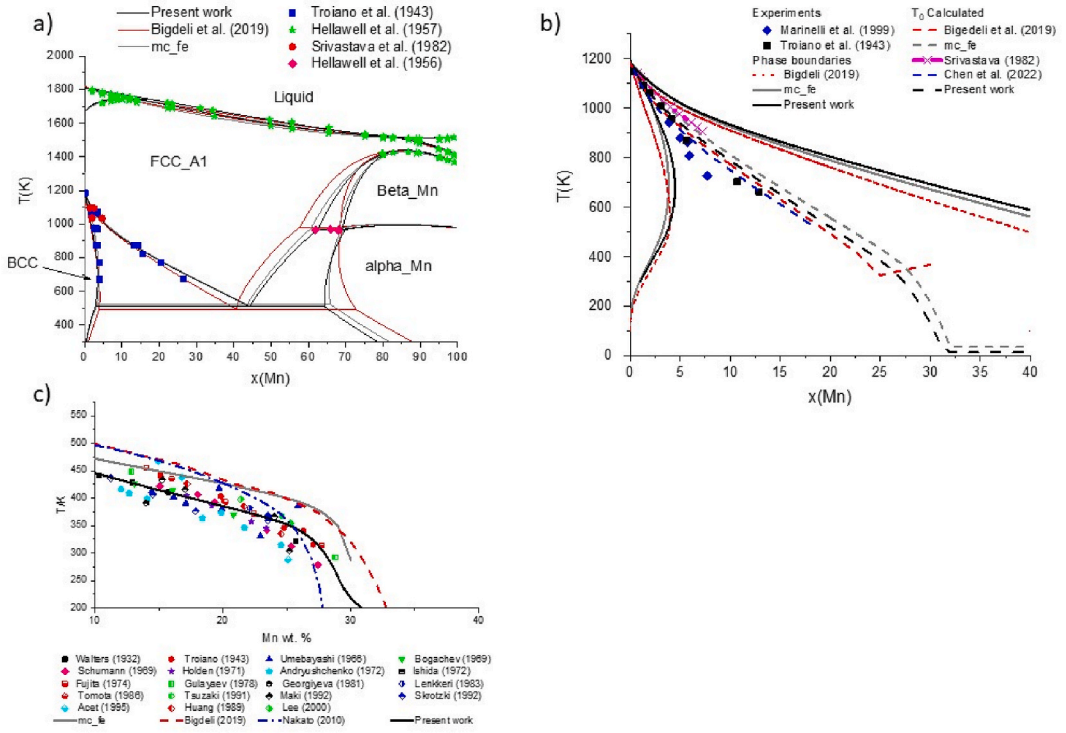

Fig. 12. Calculation in the Fe–Mn system a) Phase diagram compared to experiments [61,63,86], b) calculation of T_0 for the transformation FCC to BCC compared to Refs. [21,61], and c) T_0 for the transformation FCC to HCP [62–79].

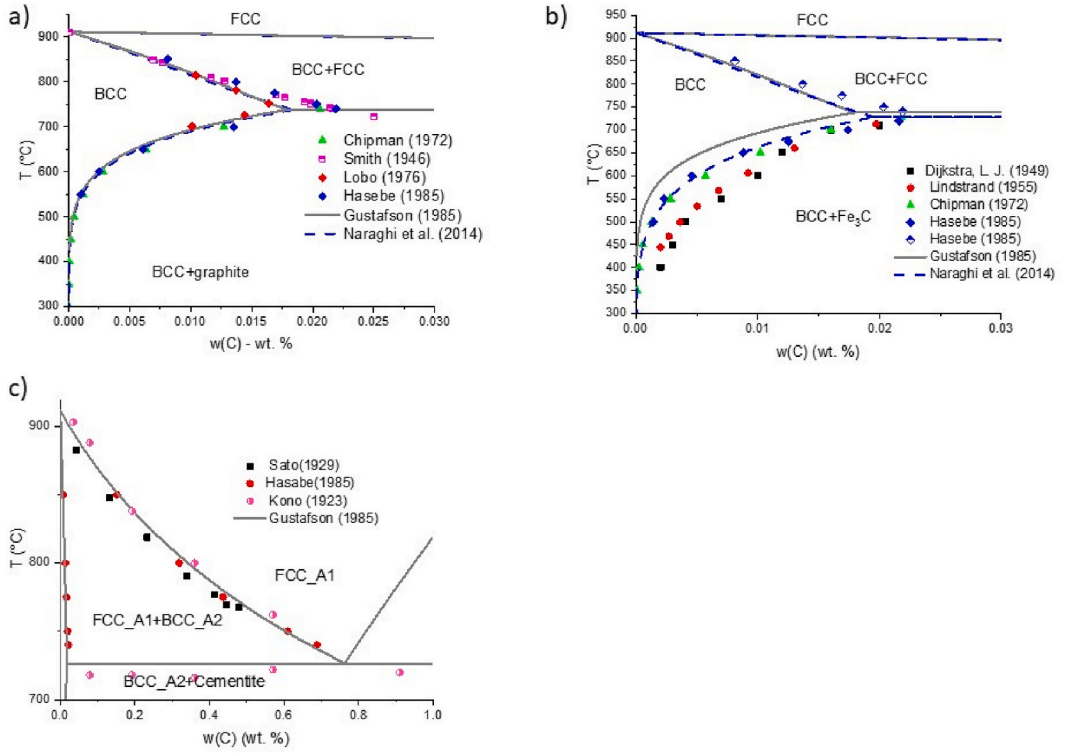

Fig. 13. Results of the Fe–C phase diagram calculation from Gustafson [36] at low temperature in the Fe-rich corner compared to experimental information [95, 100–104] and thermodynamic modeling from Naraghi et al. [37].

multi-component databases (Fig. 13). Several thermodynamic descriptions [95–97] have been proposed before the one of Gustafson [36], while, since then, the amount of revision of the thermodynamic modeling is limited [37,98]. Okamoto [99] made a compilation of the Fe–C descriptions until 1992. Naraghi et al. [37] fully revised the thermodynamic modeling of the system. Their reassessment is based on the 3rd generation of the Calphad database development. While the thermodynamic modeling of Gustafson is indeed accurate in terms of

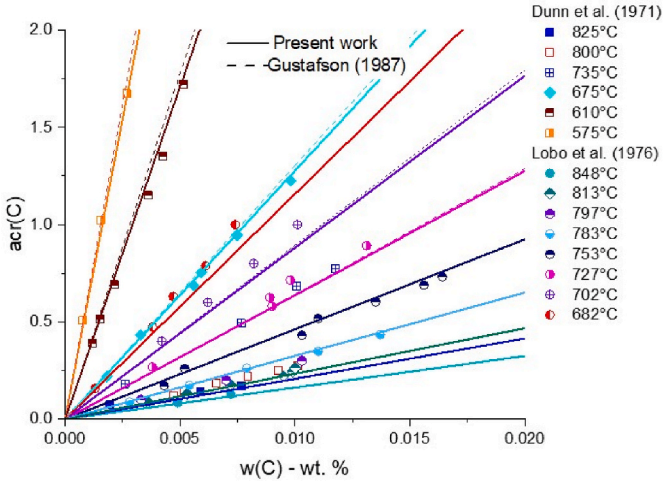

Fig. 14. Calculated activities in BCC compared to experiments [101,106], and previous thermodynamic modeling by Gustafson [36], which is implemented in the original mc_fe database.

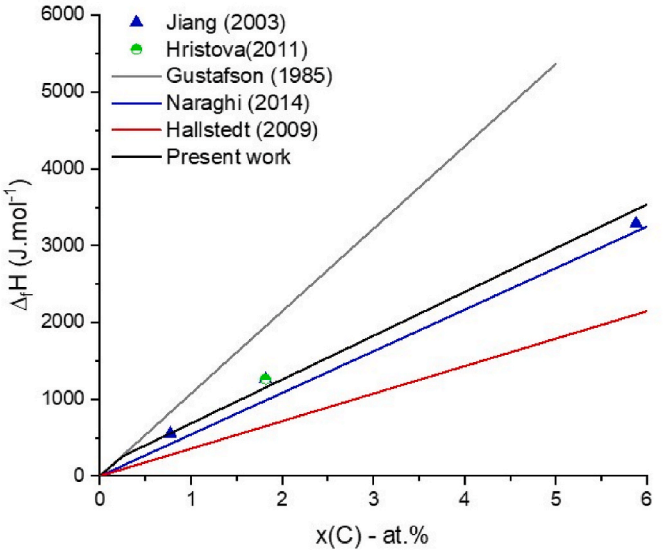

Fig. 15. Calculated enthalpy of formation at T = 298 K in BCC Fe–C compared to DFT at T = 0 K [107,108] and previous thermodynamic modeling [36, 98,109].

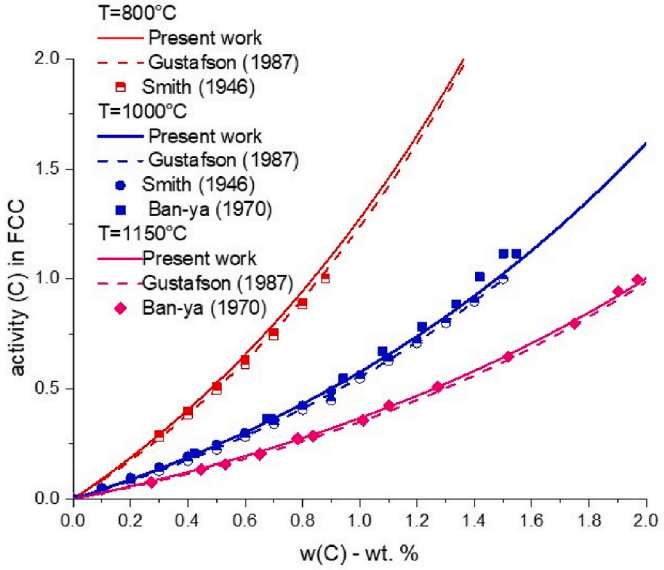

Fig. 17. The calculated activity of Carbon in FCC compared to experiments [100,111].

phase boundaries and thermodynamic properties computations, its use for T_0 and T_0' (see Eq. (7)) calculations in multi-component extensions based on their description results in a deviating slope from experimental data (see Fig. 19), with increasing discrepancy found with increasing C-content.

According to Van Bohemen et al. [105], the bainite start temperature (B_s) at high C content is higher than the given calculation with the revised thermodynamic modeling of the alloy systems (see Fig. 19). Since B_s is highly dependent on the C content, it was obvious that a re-assessment of Fe–C parameters would improve the agreement between predicted and experimental transformation temperatures.

In the present reassessment of the system, the BCC phase stability at the higher temperatures was decreased by refinement of the Gustafson [36] parameter ${}^{0}L^{BCC_{A2}}_{Fe:C,Va} = -190 * T$, thus reducing the high entropic contribution to its Gibbs energy.

Further, for the revision of the C-solubility in BCC, even though the C-solubility in BCC-Fe is very low, the carbon redistribution between FCC and BCC is particularly critical for the modeling of the bainitic transformation. Activity measurements from Lobo et al. [101] and Dunn et al. [106] were used to optimize the L^0(BCC_A2,Fe:C,Va) parameter and compared to the present modeling (Fig. 14).

While the calculated activities in BCC show negligible differences from the previous optimization at the studied temperatures, the present

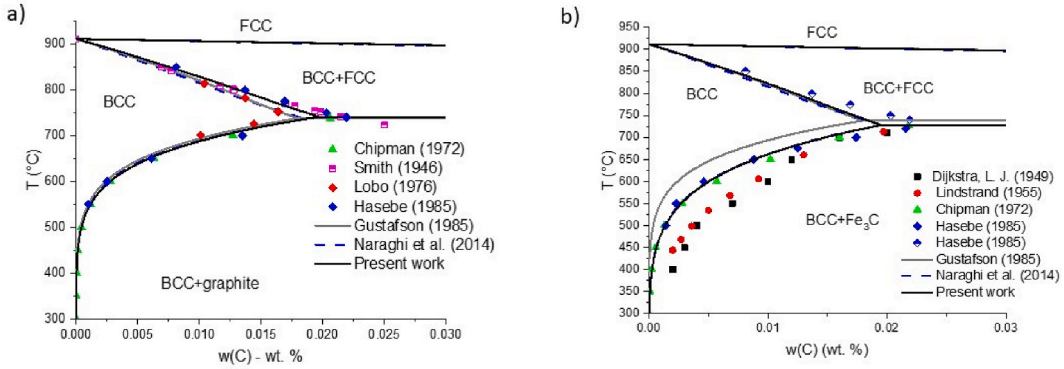

Fig. 16. Results of the Fe–C phase diagram calculation obtained from the present work at low temperature in Fe-rich compared to experimental [95,100–104] and thermodynamic modeling from Gustafson [36] and Naraghi et al. [109]. a) Equilibrium phase diagram, b) metastable phase diagram considering cementite.

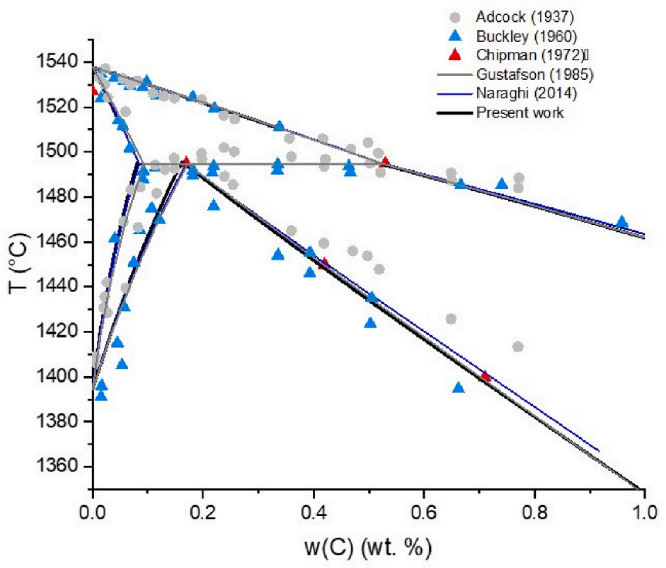

Fig. 18. Peritectic transformation in the Fe–C as calculated from the present work compared to calculations of Naraghi et al. [37] and experimental work from Refs. [95,112,113].

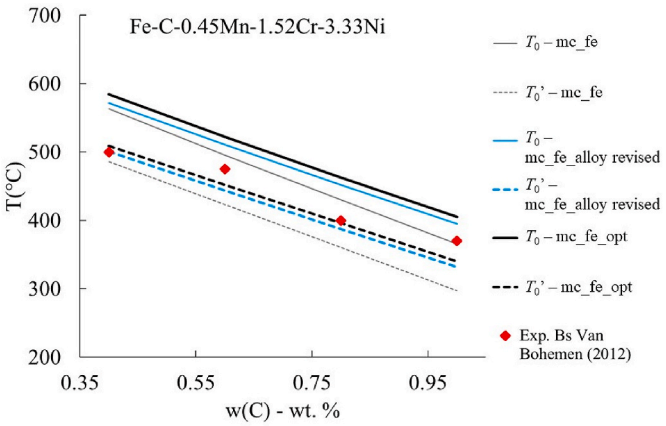

Fig. 19. Calculation of T_0 and T_0' of Fe–C-0.45Mn-1.52Cr-3.33Ni (chemical composition given in wt. %) compared to experimental data [105] from mc_fe database [9], update alloys systems (Fe–Ni, Fe–Mn, Fe–Cr) and present optimization including Fe–C.

optimization of the parameter $L^0 = +138000\text{-}283\ T$ allows suppressing the miscibility gap forming due to the parametrization suggested by Gustafson [36]. Particularly valuable low-temperature input data for a Calphad reassessment represents the enthalpy of formation of BCC by DFT analysis [107,108]. These data from Jiang et al. [107] and Hristova et al. [108] were used for the optimization in the present work. The calculated enthalpy of formation is compared to the DFT-derived $\Delta_f H$ in Fig. 15.

The regular solution model parameter G(BCC_A2,Fe:C) was then optimized to fit the experimental phase equilibria data between BCC, FCC, and graphite from Lobo [101], Chipman [95], and Smith [100]. The resulting agreement between experimental and simulated phase boundaries is good, as shown in Fig. 16a. The metastable phase diagram including cementite (Fe_3C) is compared with experiments [95,102–104] and previous thermodynamic modeling [36,109] in Fig. 17b. The parameters of cementite were adopted by Hallstedt et al. [110]. It is emphasized that the major modification of our thermodynamic modeling is given by the improved, higher solubility of C in α-Fe in the metastable Fe–C phase diagram. The higher solubility limit is consistent

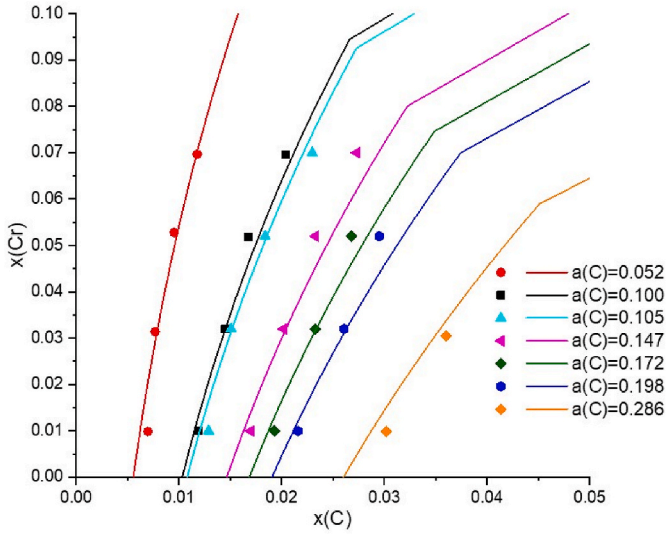

Fig. 20. Calculation of activities in FCC at T = 1000 °C in Fe–Cr–C compared to experiments [114] and modeling of Lee et al. [115].

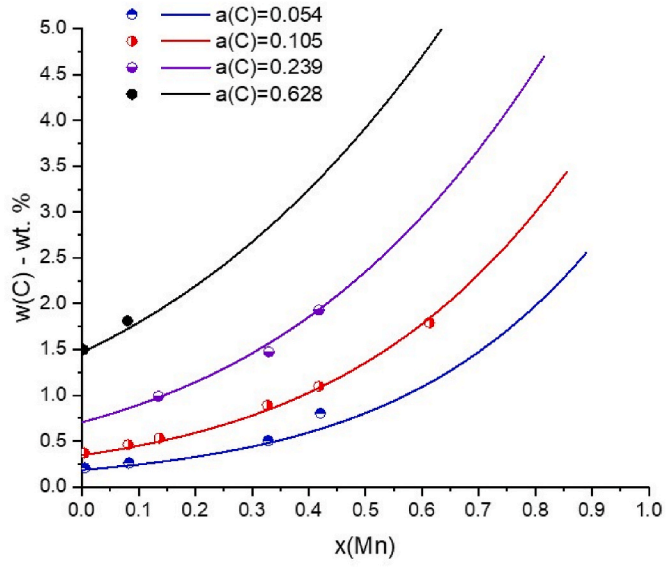

Fig. 21. Isoactivity of FCC in the Fe–Mn–C using the ternary interaction parameter of Djurovic [117] compared to experimental data of Wada et al. [118].

with the experimental data [95,100,104] and allows consistent calculations of bainite and martensite start temperatures (see Fig. 24, later).

The FCC parameters were adopted from Naraghi et al. [37] except for the temperature dependence of the G(FCC_A1,Fe:C) parameters, which were re-optimized to fit the invariant reactions. The activities in the FCC phase are shown in Fig. 17 and show consistent results with experimental data, from Refs. [100,111].

The liquid phase was slightly updated compared to the original work of Gustafson [36], i.e. $L^0_{Liquid} = -123320 + 28.5 \times T$, in order to obtain consistent phase boundaries for the solid phases in the high temperature region. The Fe–C diagram in the region of the peritectic transformation is shown in Fig. 18.

Finally, the improved results of B_s using the newly optimized parameters for Fe–Ni, Fe–Mn, Fe–Cr, and Fe–C provide consistent calculations compared to experimental results as shown in Fig. 19.

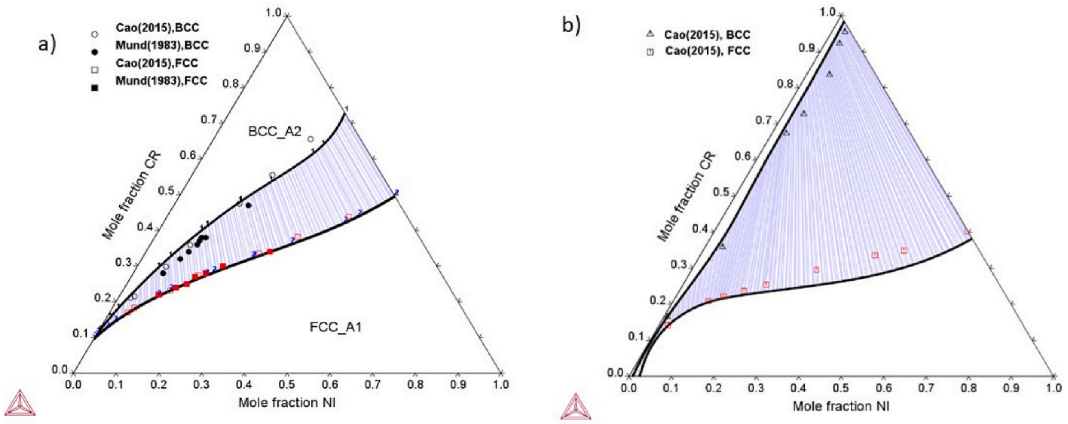

Fig. 22. Calculated isothermal section of Fe–Cr–Ni at T = 1200 °C (Fig. 22a) and T = 800 °C (Fig. 22b) compared to experimental work of Cao et al. [119] and Mund et al. [120] without consideration of the σ phase.

Chemical composition (wt. %) of the studied material from ref. [120]

Fe	C	S	P	Si	Mn	Ni	Cr	Mo
Bal.	0.15	0.003	0.006	0.24	0.51	0.17	2.47	1.11

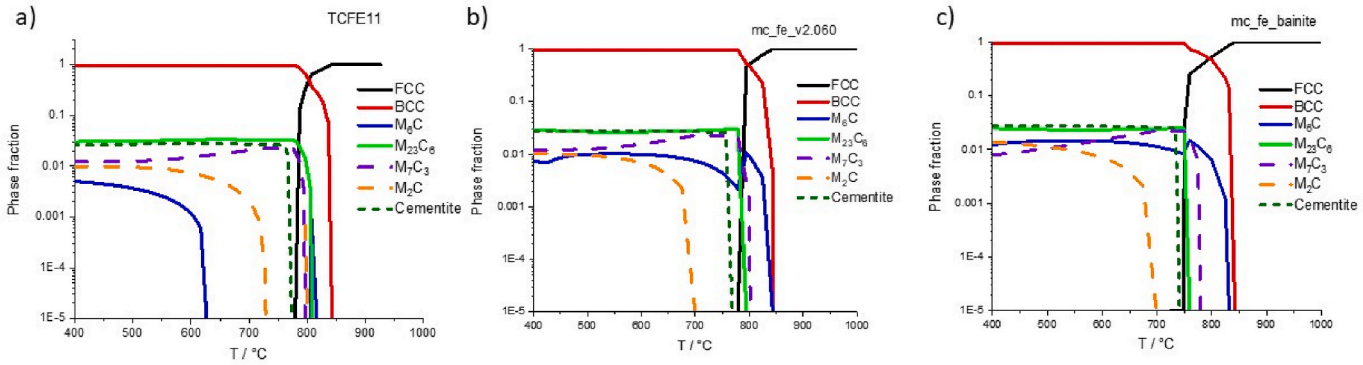

Fig. 23. Calculated phase stability of carbides (all intermetallic phases are suspended) using a) TCFE11 b) mc_fe and c) the present database mc_fe_bainite. Solid lines denote equilibrium considering all carbides, dashed lines - suspending M_6C and $M_{23}C_6$, and short-dashed lines suspending M_6C, $M_{23}C_6$, M_2C and M_7C_3.

1.3. Ternary extensions - Fe–Cr–C, Fe–Mn–C, Fe–Ni–C, Fe–Cr–Ni

The modification of the thermodynamic parameters of binary systems implies that the ternary systems will need to be revised as well. The latest thermodynamic modeling of the Fe–Cr–C system has been reported by Khvan et al. [116], where all the required experimental data are available. In consequence of the re-optimization of two binary systems, the interaction parameter of the ternary FCC phase was revised (see Appendix 1), whereas the parameter for BCC was adopted from Khvan et al. [116]. Activity data in FCC are available, and the results of the mc_fe with updated binaries Fe–C and Fe–Cr are plotted in Fig. 20 and compared to experimental data from Nishiwaza [114].

The latest thermodynamic modeling of the Fe–Mn–C is given by Djurovic et al. [117], and the influences due to our modification of the Fe–Mn and Fe–C, using the ternary parameters of Djurovic [117], were found to be negligible (see Fig. 21).

Thus, the parameters of Djurovic et al. [117] for Fe–Mn–C were adopted in the present work, since, as shown in Fig. 21, this allowed for a perfect fit with the experimental results of Wada et al. [118].

In consequence of the revision of the binary alloy systems Fe–Cr and Fe–Ni, it was necessary to re-adjust the parameters in the ternary Fe–Cr–Ni BCC and FCC phases. The calculated phase diagram is given in Fig. 22. The present work does not consider the intermetallic phase σ, since it is not in the scope of the present work, and the phase will not show up in the relatively dilute applications of bainitic and martensitic

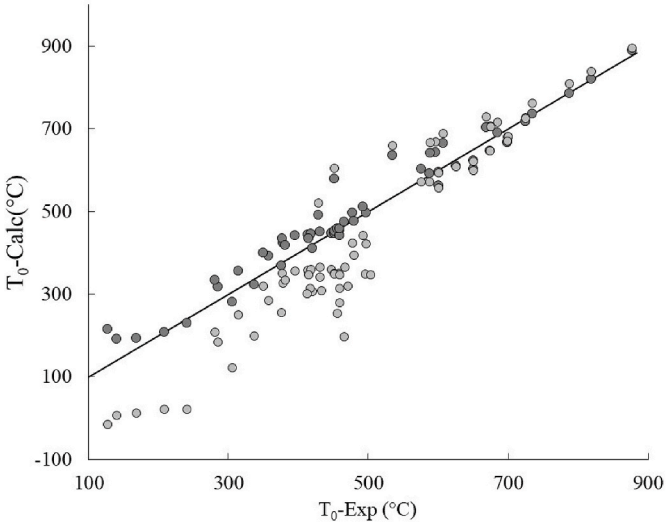

Fig. 24. Calculated T_0 using the re-assessed mc_fe database of this study (full symbols) compared to the original mc_fe [9] (empty symbols) compared to experimental data [40–43].

steels. A full optimization considering multi-component extension with applications to higher alloying has been reported by the present authors in a previous publication [121].

1.4. Consequences of the re-optimization of the sub-systems on multi-component thermodynamic databases

The current thermodynamic database was developed with the specific purpose of improving the description of the low temperature part of the Gibbs energy. Nevertheless, the thermodynamic database mc_fe [9,11] had been previously designed for several applications and provides already good benchmark with experimental findings [122]. These authors demonstrated predictive calculations of the carbide stability with a previous version of the mc_fe in a multi-component alloy, being consistent with their findings. The formation of carbides may play an important role in many martensitic and bainitic steel grades. Thus, using the developed database of this study, the stability of carbide phases in multi-component is critically compared to previous calculations [122] (Fig. 23).

Within the present work, the parameter $L^0_{M7C3}(Cr, Fe : C)$ was optimized considering the DFT calculation of Zhang et al. [123] and is set to -32045-10T, which gives a calculated $\Delta_f H = -12.64$ kJ mol^{-1} in good agreement with the DFT given at -11.4 kJ mol^{-1}. In addition, the parameters of the $M_{23}C_6$ phase in the Cr–Fe–C system were revised to keep the same solubility limit as in the previous version of the mc_fe database (see Appendix A for parameters). The present calculations are compared to the Fe-database TCFE11 of Thermocalc® offering a benchmark point (Fig. 23). In general, the computed stability of the carbides shows similar trends except for M_6C. Note that the difference in M_6C stability between TCFE11 (Thermocalc steel database) and MatCalc mc_fe shown in Fig. 23 is due to a revised sublattice description of the phase, which has been implemented in mc_fe. While TCFE11 predicts a gap of its occurrence, with a "first" dissolution around T = 620 °C, and re-appearance around T = 810 °C, replacing dissolved $M_{23}C_6$ in a very narrow temperature range. The mc_fe_v2.060 and mc_fe_bainite suggests that M_6C would be continuously stable from low temperatures up to T∼840 °C with an even increased phase fraction after $M_{23}C_6$ has dissolved. This stability issue of M_6C is not clear to date but requires further research. Typically, carbide formation and transformations between $M_{23}C_6$, M_6C, and M_7C_3 are complex. Often, non-equilibrium phase stabilities are conserved, and it is difficult to decide on the correct equilibrium state of carbides and a steel treatment to reach an unambiguous equilibrium below the austenitization temperatures. This difficulty is even increased due to complex microstructures, heterogeneities, and carbon partitioning.

Fig. 24 summarizes the improved agreement of the computed T_0 temperatures of different binary and ternary systems with the reassessed steel database of this study.

The present re-assessment of important Fe-containing sub-systems of the multi-component steel database mc_fe is one of the cornerstones for the predictive simulation of the bainite phase transformation, which finally includes kinetic aspects of C redistribution and C-trapping, too [124]. The corresponding computation of bainite start temperatures will be provided in a separate publication, which is based on the thermodynamic data developed here.

2. Conclusion

In the present work, we focused on the re-assessment of Fe-containing binary and ternary sub-systems of the Fe, C, Cr, Mn, Ni, Al, and Si steel database, to improve the computation of T_0, as well as bainite and martensite start temperatures. It was confirmed that the magnetic contribution to the Gibbs energies of alloy solution phases represents a key to a consistent dataset for the reproduction of the low and intermediate temperature part of the binary and ternary phase diagrams, thermodynamic properties, and T_0 lines with transition elements.

The Fe–C system was revised to improve the solubility of C into ferrite, which plays a decisive role in bainite modeling.

As consequence on the revision of the binary systems, ternary parameters were re-optimized or edited to more recent publications. We present here a complete thermodynamic parameter set of the Fe-rich region of the multi-component steel system Fe–Cr–Ni–Mn–Al–Si–C, which can be used for computational thermodynamics from room temperature up to high temperatures close to the solidus, and in a mean-field or full field approach for predictive kinetic simulation.

Declaration of competing interest

The authors declare that they have no known competing financial interests or personal relationships that could have appeared to influence the work reported in this paper.

Data availability

Data will be made available on request.

Acknowledgments

The authors gratefully acknowledge the financial support under the scope of the COMET program within the K2 Center "Integrated Computational Material, Process and Product Engineering (IC-MPPE)" (Project No 859480). This program is supported by the Austrian Federal Ministries for Climate Action, Environment, Energy, Mobility, Innovation and Technology (BMK) and for Digital and Economic Affairs (BMDW), represented by the Austrian research funding association (FFG), and the federal states of Styria, Upper Austria and Tyrol.

Appendix A. Supplementary data

Supplementary data to this article can be found online at https://doi.org/10.1016/j.calphad.2023.102531.

References

[1] G. Ghosh, G.B. Olson, Computational thermodynamics and the kinetics of martensite transformation, J. Phase Equil. 22 (2001) 199–207, https://doi.org/10.1361/105497101770338653.
[2] M. Palumbo, Thermodynamics of martensitic transformations in the framework of the CALPHAD approach, Calphad 32 (2008) 693–708, https://doi.org/10.1016/j.calphad.2008.08.006.
[3] L. Leach, P. Kolmskog, L. Höglund, M. Hillert, A. Borgenstam, Use of Fe-C information as reference for alloying effects on BS, Metall. Mater. Trans. 50 (2019) 4531–4540, https://doi.org/10.1007/s11661-019-05371-1.
[4] M. Hillert, Critical limit for massive transformation, Mettalurgical Mater. Transations A. 33 (2002) 2299–2308, https://doi.org/10.1007/s11661-002-0353-5.
[5] L. Kaufman, M. Cohen, Thermodynamics and kinetics of martensitic transformations, Prog. Met. Phys. 7 (1958) 165–246, https://doi.org/10.1016/0502-8205(58)90005-4.
[6] H.K.D.H. Bhadeshia, Bainite in Steels Theory and Practice, third ed., 2019, https://doi.org/10.1201/9781315096674.
[7] H. Chen, W. Xu, Q. Luo, Q. Li, Y. Zhang, J. Wang, K.-C. Chou, Thermodynamic prediction of martensitic transformation temperature in Fe-C-X (X=Ni, Mn, Si, Cr) systems with dilatational coefficient model, J. Mater. Sci. Technol. 112 (2022) 291–300, https://doi.org/10.1016/j.jmst.2021.09.060.
[8] A. Borgenstam, M. Hillert, Driving force for f.c.c->b.c.c martensites in Fe-X alloys, Acta Mater. 45 (1997) 2079–2091, https://doi.org/10.1016/S1359-6454(96)00308-4.
[9] E. Povoden-Karadeniz, mc_fev2.060 (2020). https://www.matcalc.at/index.php/databases/open-da.
[10] E. Kozeschnik, Mean-Field kinetics modeling, in: Encycl. Mater. Met. Alloy, 2022, pp. 521–526.
[11] A. Jacob, C. Domain, G. Adjanor, P. Todeschini, E. Povoden-karadeniz, Thermodynamic modeling of G-phase and assessment of phase stabilities in reactor pressure vessel steels and cast duplex stainless steels, J. Nucl. Mater. 533 (2020), https://doi.org/10.1016/j.jnucmat.2020.152091.

[12] H. Lukas, S.G. Fries, B. Sundman, Computational Thermodynamics the Calphad Method, Cambridge university press, 2007, https://doi.org/10.1017/CBO9780511804137.

[13] J.O. Andersson, T. Helander, L. Höglund, P. Shi, B. Sundman, Thermo-Calc & DICTRA, computational tools for materials science, Calphad 26 (2002) 273–312, https://doi.org/10.1016/S0364-5916(02)00037-8.

[14] N. Saunders, Z. Guo, X. Li, A.P. Miodownik, J.P. Schillé, Using JMatPro to model materials properties and behavior, JOM (J. Occup. Med.) 55 (2003) 60–65, https://doi.org/10.1007/s11837-003-0013-2.

[15] W. Cao, S.L. Chen, F. Zhang, K. Wu, Y. Yang, Y.A. Chang, R. Schmid-Fetzer, W. A. Oates, PANDAT software with PanEngine, PanOptimizer and PanPrecipitation for multi-component phase diagram calculation and materials property simulation, Calphad Comput. Coupling Phase Diagrams Thermochem. 33 (2009) 328–342, https://doi.org/10.1016/j.calphad.2008.08.004.

[16] A.T. Dinsdale, SGTE data for pure elements, Calphad 15 (1991) 317–425, https://doi.org/10.1016/0364-5916(91)90030-N.

[17] A. Janz, R. Schmid-Fetzer, Impact of ternary parameters, Calphad 29 (2005) 37–39, https://doi.org/10.1016/j.calphad.2005.01.003.

[18] M. Hillert, J. Magnus, A model for alloying effects in ferromagnetic metals, Calphad 2 (1978) 227–238, https://doi.org/10.1016/0364-5916(78)90011-1.

[19] W. Xiong, H. Zhang, L. Vitos, M. Selleby, Magnetic phase diagram of the Fe-Ni system, Acta Mater. 59 (2011) 521–530, https://doi.org/10.1016/j.actamat.2010.09.055.

[20] G. Cacciamani, A. Dinsdale, M. Palumbo, A. Pasturel, The Fe-Ni system: thermodynamic modelling assisted by atomistic calculations, Intermetallics 18 (2010) 1148–1162, https://doi.org/10.1016/j.intermet.2010.02.026.

[21] S. Bigdeli, M. Selleby, A thermodynamic assessment of the binary Fe-Mn system for the third generation of Calphad databases, Calphad 64 (2019) 185–195, https://doi.org/10.1016/j.calphad.2018.11.011.

[22] A. Gabriel, P. Gustafson, I. Ansara, A thermodynamic evaluation of the C-Fe-Ni system, Calphad 11 (1987) 203–218, https://doi.org/10.1016/0364-5916(87)90039-3.

[23] I. Ohnuma, S. Shimenouchi, T. Omori, K. Ishida, R. Kainuma, Experimental determination and thermodynamic evaluation of low-temperature phase equilibria in the Fe–Ni binary system, Calphad 67 (2019), 101677, https://doi.org/10.1016/j.calphad.2019.101677.

[24] W. Huang, Thermodynamic properties of the Fe-Mn-V-C system, Metall. Mater. Trans. 22A (1991) 1911–1920.

[25] J.O. Andersson, B. Sundman, Thermodynamic properties of the CrFe system, Calphad 11 (1987) 83–92, https://doi.org/10.1016/0364-5916(87)90021-6.

[26] W. Xiong, M. Selleby, Q. Chen, J. Odqvist, Y. Du, Phase equilibria and thermodynamic properties in the Fe-Cr system, Crit. Rev. Solid State Mater. Sci. 35 (2010) 125–152, https://doi.org/10.1080/10408431003788472.

[27] W. Xiong, P. Hedström, M. Selleby, J. Odqvist, M. Thuvander, Q. Chen, An improved thermodynamic modeling of the Fe–Cr system down to zero kelvin coupled with key experiments, Calphad 35 (2011) 355–366, https://doi.org/10.1016/j.calphad.2011.05.002.

[28] A. Jacob, E. Povoden-Karadeniz, E. Kozeschnik, Revised thermodynamic description of the Fe-Cr system based on an improved sublattice model of the σ phase, Calphad Comput. Coupling Phase Diagrams Thermochem. 60 (2018) 16–28, https://doi.org/10.1016/j.calphad.2017.10.002.

[29] P. Lafaye, C. Toffolon-Masclet, J.C. Crivello, J.M. Joubert, Experimental study, first-principles calculation and thermodynamic modelling of the Cr–Fe–Nb–Sn–Zr quinary system for application as cladding materials in nuclear reactors, J. Nucl. Mater. 544 (2021), 152692, https://doi.org/10.1016/j.jnucmat.2020.152692.

[30] J. Lacaze, B. Sundman, An assessment of the Fe-C-Si system, Metall. Trans. A 22 (1991) 2211–2223, https://doi.org/10.1007/BF02664987.

[31] I. Ohnuma, S. Abe, S. Shimenouchi, T. Omori, R. Kainuma, K. Ishida, Experimental and thermodynamic studies of the Fe–Si binary system, ISIJ Int. 52 (2012) 540–548, https://doi.org/10.2355/isijinternational.52.540.

[32] Y. Yuan, F. Pan, D. Li, A. Watson, The re-assessment of the Mg-Zn and Fe-Si systems and their incorporation in thermodynamic descriptions of the Al-Mg-Zn and Fe-Si-Zn systems, Calphad 44 (2014) 54–61, https://doi.org/10.1016/j.calphad.2013.07.007.

[33] S. Cui, I.H. Jung, Critical reassessment of the Fe-Si system, Calphad 56 (2017) 108–125, https://doi.org/10.1016/j.calphad.2016.11.003.

[34] N. Saunders, COST 507: Thermochemical Database for Light Metal Alloys, 1998.

[35] M. Rank, P. Franke, H.J. Seifert, Thermodynamic investigations in the Al–Fe system: thermodynamic modeling using CALPHAD, Int. J. Mater. Res. 110 (2019) 406–421, https://doi.org/10.3139/146.111765.

[36] P. Gustafson, A thermodynamic evaluation of the Fe-C system, Scand. J. Metall. 14 (1985) 259–267.

[37] R. Naraghi, M. Selleby, J. Ågren, Thermodynamics of stable and metastable structures in Fe-C system, Calphad Comput. Coupling Phase Diagrams Thermochem. 46 (2014) 148–158, https://doi.org/10.1016/j.calphad.2014.03.004.

[38] Z. Jicheng, J. Zhanpeng, Thermodynamics of the massive, bainitic and martensitic transformations in FeC, FeNi, FeCr and FeCu alloys, Acta Metall. Mater. 38 (1990) 425–431, https://doi.org/10.1016/0956-7151(90)90148-A.

[39] A. Jacob, B. Schuscha, P. Retzl, E. Kozeschnik, Thermodynamic Prediction of T0' Including BCT Transformation, 2022. Unpublished.

[40] Y. Liu, F. Sommer, E.J. Mittemeijer, Critical temperature for massive transformation in ultra-low-carbon Fe - C alloys, Int. J. Mater. Res. 99 (2008) 925–932, https://doi.org/10.3139/146.101730.

[41] K. Ishida, T. Nishizawa, Ferrite/Austenite stabilizing parameter of alloying elements in steel at 200~500°C, Trans Jap Inst Met 15 (1974) 217–224, https://doi.org/10.2320/matertrans1960.15.217.

[42] A.R. Troiano, F. McGuire, A study of the iron-rich iron-manganese alloys, Trans ASM 31 (1943) 340–364.

[43] P. Marinelli, A. Baruj, S. Cotes, A. Fernández Guillermet, M. Sade, The γ↔α′ martensitic transformation in Fe-Mn and Fe-Mn-Co alloys: experiments, thermodynamic analysis and systematics of driving forces, Mater. Sci. Eng. 273–275 (1999) 498–502, https://doi.org/10.1016/s0921-5093(99)00387-1.

[44] A.D. Romig, J.I. Goldstein, Determination of the Fe-Ni and Fe-Ni-P phase diagrams at low temperatures (700 to 300 °C), Metall. Trans. A 11 (1980) 1151–1159, https://doi.org/10.1007/BF02668139.

[45] C.W. Yang, D.B. Williams, J.I. Goldstein, A revision of the Fe-Ni phase diagram at low temperatures (<400 °C), J. Phase Equil. 17 (1996) 522–531, https://doi.org/10.1007/BF02665999.

[46] E.A. Owen, A.H. Sully, XXXI. On the migration of atoms in iron-nickel alloys, London, Edinburgh, Dublin Philos. Mag. J. Sci. 31 (1941) 314–338, https://doi.org/10.1080/14786444108520762.

[47] E. Scheil, E. Saftig, Messung der Umwandlungswarme hei der Martensithildung an Eisen-Nickel-Legierungen mit Hilfe einer Trockeneiskalorimeters, Arch. für das Eisenhuttenwes. 31 (1960) 623–632.

[48] R.G. Yeo, Effects of some alloying elements on transformation of Fe-22.5 pct Ni alloys, Trans AIME 227 (1963) 884.

[49] W. Xiong, Q. Chen, P.A. Korzhavyi, M. Selleby, An improved magnetic model for thermodynamic modeling, Calphad 39 (2012) 11–20, https://doi.org/10.1016/j.calphad.2012.07.002.

[50] H. Asano, Magnetism of γ Fe-Ni invar alloys with low nickel concentration, J. Phys. Soc. Japan. 27 (1969) 542–553, https://doi.org/10.1143/JPSJ.27.542.

[51] D. Bardos, J.L. Beeby, A. Aldred, Magnetic moments in body-centered cubic Fe-Ni-Al alloys, Phys. Rev. 177 (1969) 878–881, https://doi.org/10.1103/PhysRev.177.878.

[52] K. Sumiyama, M. Kadono, Y. Nakamura, Metastable bcc phase in sputtered Fe-Ni alloys, Trans. Japan Inst. Met. 24 (1983) 190–194.

[53] R.A. Reck, D.L. Fry, Orbital and spin magnetization in Fe-Co, Fe-Ni, and Ni-Co, Phys. Rev. 184 (1969) 492–495, https://doi.org/10.1103/PhysRev.184.492.

[54] R.J. Wackelin, E.L. Yates, A study of the order-disorder transformation in iron-nickel alloys in the region FeNi3, Proc. Phys. Soc. B 66 (1953) 221–240, https://doi.org/10.1088/0370-1301/66/3/310.

[55] M. Peschard, Rev. Métall. 22 (1925) 663. No Title.

[56] C. Wu, B.J. Lee, X. Su, Modified embedded-atom interatomic potential for Fe-Ni, Cr-Ni and Fe-Cr-Ni systems, Calphad 57 (2017) 98–106, https://doi.org/10.1016/j.calphad.2017.03.007.

[57] W.A. Dench, Adiabatic high-temperature calorimeter for the measurement of heats of alloying, Trans. Faraday Soc. 59 (1963).

[58] Y. Wang, K. Li, F. Soisson, C.S. Becquart, Combining DFT and CALPHAD for the development of on-lattice interaction models: the case of Fe-Ni system, Phys. Rev. Mater. 4 (2020) 1–13, https://doi.org/10.1103/PhysRevMaterials.4.113801.

[59] L. Kaufman, M. Cohen, The martensitic transformation in the iron-nickel system, JOM (J. Occup. Med.) 8 (1956) 1393–1401, https://doi.org/10.1007/bf03377892.

[60] C.E. Campbell, Ph.D. Thesis, Northwestern University, 1997.

[61] K.K. Srivastava, J.S. Kirkaldy, The Alph-Gamm Phase boundaries and the T0 line for the Fe-Mn alloys, Metall. TRan. 13 (1982) 2113–2119.

[62] F. Walters Jr., M. Gensamer, Trans. Am. Soc. Met. 19 (1932) 608. No Title.

[63] A. Troiano, F. McGuire, A.R McGuire Troiano, F.T, Trans, Am. Soc. Met. 31 (1943) 340.

[64] H. Umebayashi, Y. Ishikawa, Antoferromagnetism of g Fe-Mn alloys, J. Phys. Soc. Japan. 21 (1966) 1281–1294.

[65] I. Bogachev, V.F. Yegolayev, G.Y. Zvigintseva, L.V. Zhuravel, Phys. Met. Metallogr. 28 (1969) 125. No Title.

[66] H. Schumann, Die hexagonale epsilon phase in eisen und eisenlegierungen, Arch Eisenhuettenw 40 (1969) 1027–1037.

[67] A. Holden, J.D. Bolton, E.R. Petty, J. Iron Steel Inst. 209 (1971) 156. No Title.

[68] I. Andryushchenko, L.Y. Georgiyeva, Phys. Met. Metallogr. 33 (1972) 156. No Title.

[69] K. Ishida, J. Nishizawa, Effect of Alloying elements on the stability of epsilon iron, J. Japan Inst. Met. Mater. 36 (1972) 1238.

[70] M. Fujita, I. Uchiyama, Tetsu-To-Hagane 60 (1974) 525. No Title.

[71] A. Gulayaev, T. Volynova, I.Y. Georgieva, Met. Sci. Heat Treat. 20 (1978) 179. No Title.

[72] I.Y. Georgiyeva, N.A. Soronika, V.I. Gal'tsova, Phys. Met. Metallogr. 49 (1981) 178. No Title.

[73] J. Lenkkeri, J. Levoska, Philos. Mag. A 48 (1983) 749. No Title.

[74] Y. Tomota, M. Strum, J.W. Morris, Met. Trans. 17A (1986) 537. No Title.

[75] K. Tsuzaki, S. Fukasaku, Y. Tomota, T. Maki, Mater. Mater. Trans. JIM. 32 (1991) 222. No Title.

[76] T. Maki, K. Tsuzaki, Proc. ICOMAT-92, Monterey Inst. Adv. Stud. 17A (1992) 1151. No Title.

[77] W. Huang, Thermodynamic properties of the Fe-Mn-V-C system, Met. Trans. A. 22 (1911–1920) n.d.

[78] Y.K. Lee, C. Choi, Met. Trans. 31A (2000) 335. No Title.

[79] J. Nakano, P.J. Jacques, Effects of the thermodynamic parameters of the hcp phase on the stacking fault energy calculations in the Fe-Mn and Fe-Mn-C systems, Calphad 34 (2010) 167–175, https://doi.org/10.1016/j.calphad.2010.02.001.

[80] V.T. Witusiewicz, F. Sommer, E.J. Mittemeijer, Enthalpy of formation and heat capacity of Fe-Mn alloys, Metall. Mater. Trans. B Process Metall. Mater. Process. Sci. 34 (2003) 209–223, https://doi.org/10.1007/s11663-003-0008-y.
[81] T. Schneider, M. Rellinghaus, E.F. Wassermann, W. Pepperhoff, Antiferromagnetic Invar and anti invar Fe-Mn alloys, Phys. Rev. B 51 (1995) 8917–8921.
[82] V.T. Witusiewicz, F. Sommer, E.J. Mittemeijer, Reevaluation of the Fe-Mn phase diagram, J. Phase Equilibria Diffus. 25 (2004) 346–354, https://doi.org/10.1361/15477030420115.
[83] Y.M. Kim, Y.H. Shin, B.J. Lee, Modified embedded-atom method interatomic potentials for pure Mn and the Fe-Mn system, Acta Mater. 57 (2009) 474–482, https://doi.org/10.1016/j.actamat.2008.09.031.
[84] A. Schneider, C.C. Fu, O. Waseda, C. Barreteau, T. Hickel, Ab initio based models for temperature-dependent magnetochemical interplay in bcc Fe-Mn alloys, Phys. Rev. B 103 (2021), 24421, https://doi.org/10.1103/PhysRevB.103.024421.
[85] C. Paduani, E. Galvao da Silva, G.A. Perez-Alcazar, M. McElfresh, Mössbauer effect and magnetization studies of a-FeMn alloys, J. Appl. Phys. 12 (1991) 7524–7531, https://doi.org/10.1016/j.actamat.2005.02.042.
[86] A. Hellawell, W. Hume-Rothery, The constitution of alloys of iron and manganese with transition elements of the first long period, Philos. Trans. R. Soc. London. Ser. A, Math. Phys. Sci. 249 (1957) 417–459, https://doi.org/10.1098/rsta.1957.0004.
[87] A. Jacob, E. Povoden-Karadeniz, E. Kozeschnik, Revised thermodynamic description of the Fe-Cr system based on an improved sublattice model of the σ phase, Calphad 60 (2018) 16–28, https://doi.org/10.1016/j.calphad.2017.10.002.
[88] J. Miettinen, Reassessed thermodynamic solution phase data for ternary Fe-Si-C system, Calphad 22 (1998) 231–256, https://doi.org/10.1016/S0364-5916(98)00026-1.
[89] Y. Yuan, F. Pan, D. Li, A. Watson, The re-assessment of the Mg–Zn and Fe–Si systems and their incorporation in thermodynamic descriptions of the Al–Mg–Zn and Fe–Si–Zn systems, Calphad 44 (2014) 54–61, https://doi.org/10.1016/j.calphad.2013.07.007.
[90] S. Cui, I.H. Jung, Critical reassessment of the Fe-Si system, Calphad 56 (2017) 108–125, https://doi.org/10.1016/j.calphad.2016.11.003.
[91] B. Sundman, I. Ohnuma, N. Dupin, U.R. Kattner, S.G. Fries, An assessment of the entire Al-Fe system including D03 ordering, Acta Mater. 57 (2009) 2896–2908, https://doi.org/10.1016/j.actamat.2009.02.046.
[92] W. Zheng, S. He, M. Selleby, Y. He, L. Li, X.G. Lu, J. Ågren, Thermodynamic assessment of the Al-C-Fe system, Calphad 58 (2017) 34–49, https://doi.org/10.1016/j.calphad.2017.05.003.
[93] B. Hallstedt, A.V. Khvan, B.B. Lindahl, M. Selleby, S. Liu, PrecHiMn-4—a thermodynamic database for high-Mn steels, Calphad Comput, Coupl. Phase Diagr. Thermochem. 56 (2017) 49–57, https://doi.org/10.1016/j.calphad.2016.11.006.
[94] J. yu Tian, G. Xu, M. xing Zhou, H. jiang Hu, Z. liang Xue, Effects of Al addition on bainite transformation and properties of high-strength carbide-free bainitic steels, J. Iron Steel Res. Int. 26 (2019) 846–855, https://doi.org/10.1007/s42243-019-00253-7.
[95] J. Chipman, Thermodynamics and phase diagram of the Fe-C system, Metall. Trans. A 3 (1972) 55–64, https://doi.org/10.1007/BF02680585.
[96] J. Agren, A thermodynamic analysis of the Fe-C and the Fe-N phase diagrams, Metall. Trans. A 10 (1979) 1847–1852, https://doi.org/10.1007/BF02662408.
[97] H. Ohtani, M. Hasebe, T. Nishizawa, Calculation of Fe-C, Co-C and Ni-C phase diagrams, Trans. Iron Steel Inst. Japan. 24 (1984) 857–864, https://doi.org/10.2355/isijinternational1966.24.857.
[98] B. Hallstedt, D. Djurovic, Modelling of interstitials in the bcc phase, Calphad 33 (2009) 233–236, https://doi.org/10.1016/j.calphad.2008.09.013.
[99] H. Okamoto, The C-Fe (carbon-iron) system, J. Phase Equil. 13 (1992) 543–565, https://doi.org/10.1007/BF02665767.
[100] R.P. Smith, Equilibrium of iron-carbon alloys with mixtures of CO-CO2 and CH4-H2, J. Am. Chem. Soc. 68 (1946) 1163–1175, https://doi.org/10.1021/ja01211a010.
[101] J.A. Lobo, G.H. Geiger, Thermodynamics and solubility of carbon in ferrite and ferritic Fe-Mo alloys, Metall. Trans. A 7 (1976) 1347–1357, https://doi.org/10.1007/BF02658820.
[102] L.J. Dijkstra, Precipitation phenomena in the solid solutions of nitrogen and carbon in alpha iron below the eutectoid temperature, JOM (J. Occup. Med.) 1 (1949) 252–260, https://doi.org/10.1007/bf03398106.
[103] E. Lindstrand, A method for the measurement of elastic relaxation, and its use for determination of the solubility of carbon in α-iron, Acta Metall. 3 (1955) 431–435, https://doi.org/10.1016/0001-6160(55)90130-9.
[104] M. Hasebe, H. Ohtani, T. Nishizawa, Effect of magnetic transition on solubility of carbon in bcc Fe and fee Co-Ni alloys, Metall. Trans. A 16 (1985) 913–921, https://doi.org/10.1007/BF02814843.
[105] S.M.C. Van Bohemen, Bainite and martensite start temperature calculated with exponential carbon dependence, Mater. Sci. Technol. 28 (2012) 487–495, https://doi.org/10.1179/1743284711Y.0000000097.
[106] W.W. Dunn, R.B. McLellan, The thermodynamic properties of carbon in body-centered cubic iron, Metall. Trans. A 2 (1971) 1079–1086, https://doi.org/10.1007/BF02664239.
[107] D.E. Jiang, E.A. Carter, Carbon dissolution and diffusion in ferrite and austenite from first principles, Phys. Rev. B Condens. Matter 67 (2003) 1–11, https://doi.org/10.1103/PhysRevB.67.214103.
[108] E. Hristova, R. Janisch, R. Drautz, A. Hartmaier, Solubility of carbon in α-iron under volumetric strain and close to the Σ5(3 1 0)[0 0 1] grain boundary: comparison of DFT and empirical potential methods, Comput. Mater. Sci. 50 (2011) 1088–1096, https://doi.org/10.1016/j.commatsci.2010.11.006.
[109] R. Naraghi, M. Selleby, J. Ågren, Thermodynamics of stable and metastable structures in Fe-C system, Calphad 46 (2014) 148–158, https://doi.org/10.1016/j.calphad.2014.03.004.
[110] B. Hallstedt, D. Djurovic, J. von Appen, R. Dronskowski, A. Dick, F. Körmann, T. Hickel, J. Neugebauer, Thermodynamic properties of cementite (Fe3C), Calphad 34 (2010) 129–133, https://doi.org/10.1016/j.calphad.2010.01.004.
[111] S. Ban-ya, J.F. Elliott, J. Chipman, Thermodynamics of austenitic Fe-C alloys, Metall. Mater. Trans. 1 (1970) 1313–1320, https://doi.org/10.1007/BF02900248.
[112] F. Adcock, An investigation of the iron-carbon constitutional diagram, Part. I Preliminary survey of the d region, J. Iron Steel Inst. 135 (1937) 281–292.
[113] R. Buckley, W. Hume-Rothery, Liquidus and solidus relations in iron-rich iron–carbon alloys, J. Iron Steel Inst. 196 (1960) 403–406.
[114] T. Nishizawa, Experimental study of the Fe-Mn and Fe-Mn-C and Fe-Cr-C systems at 1000 degree C, Scand. J. Metall. 6 (1977) 74–78.
[115] B.J. Lee, On the stability of Cr-carbides, Calphad 16 (1992) 121–149.
[116] A.V. Khvan, B. Hallstedt, C. Broeckmann, A thermodynamic evaluation of the Fe-Cr-C system, Calphad Comput, Coupl. Phase Diagr. Thermochem. 46 (2014) 24–33, https://doi.org/10.1016/j.calphad.2014.01.002.
[117] D. Djurovic, B. Hallstedt, J. von Appen, R. Dronskowski, Thermodynamic assessment of the Fe–Mn–C system, Calphad 35 (2011) 479–491, https://doi.org/10.1016/j.calphad.2011.08.002.
[118] T. Wada, H. Wada, J.F. Elliott, J. Chipman, Thermodynamics of the fcc Fe-Mn-C and Fe-Si-C alloys, Metall. Trans. A 3 (1972) 1657–1662, https://doi.org/10.1007/bf02643059.
[119] S. Cao, J.-C. Zhao, Application of dual-anneal diffusion multiples to the effective study of phase diagrams and phase transformations in the Fe–Cr–Ni system, Acta Mater. 88 (2015) 196–206, https://doi.org/10.1016/j.actamat.2014.12.027.
[120] R. Mundt, H. Hoffmeister, a-g phase equilibria in iron-rich iron-chromium-nickel alloys at temperature between 1200 and 1350°C, Arch. für das Eisenhuttenwes. 54 (1983) 253–256.
[121] A. Jacob, E. Povoden-Karadeniz, Predictive computations of intermetallic σ phase evolution in duplex steel. I) Thermodynamic modeling of σ phase in the Fe–Cr–Mn–Mo–Ni system, Calphad 71 (2020), 101810, https://doi.org/10.1016/j.calphad.2020.101998.
[122] S. Dépinoy, C. Toffolon-Masclet, S. Urvoy, J. Roubaud, B. Marini, F. Roch, E. Kozeschnik, A.F. Gourgues-Lorenzon, Carbide precipitation in 2.25 Cr-1 Mo bainitic steel: effect of heating and isothermal tempering conditions, Metall. Mater. Trans. A Phys. Metall. Mater. Sci. 48 (2017) 2164–2178, https://doi.org/10.1007/s11661-017-4045-6.
[123] D. Zhang, T. Hou, X. Liang, P. Zheng, Y. Zheng, H. Lin, K. Wu, The structura, magnetic, electronic, and mechanical properties of orthogonal/hexagonal M7C3 (M=Fe and Cr) carbides from first-ptinciples, Vacuum 3 (2022), 100310, https://doi.org/10.1016/j.vacuum.2022.111175.
[124] P. Retzl, S. Zamberger, E. Kozeschnik, Computational analysis of austenite film thickness and C-redistribution in carbide-free bainite, Mater. Res. Express 8 (2021), 76502, https://doi.org/10.1088/2053-1591/ac0d6f.